

SUPPLEMENT

Title: "A Model of Canine Purkinje Cell Electrophysiology and Ca^{2+} cycling: Rate Dependence, Triggered Activity and Comparison to Ventricular Myocyte"

Pan Li and Yoram Rudy

- I. Definitions and Abbreviations (Page 2-4)
- II. Model Parameters (Page 5-6)
- III. Model Equations and Validation (Page 7-25)
- IV. Online Figures VIII, IX, X (Page 26-27)
- V. Models Comparison Table (Page 28-29)
- VI. Supplemental References (Page 30-32)

I DEFINITIONS AND ABBREVIATIONS

| Abbreviations | Definitions |
|---------------------------------------|---|
| | General parameters |
| AP | Action Potential |
| APD ₉₀ | Action Potential Duration (at 90% repolarization) (ms) |
| CL | Cycle Length (ms) |
| DI | Diastolic Interval (ms) |
| CaT | Ca ²⁺ Transient (mmol/L) |
| PCS | Peripheral Coupling Subspace |
| SSL | Sub-Sarcolemmal Compartment |
| Myo | Bulk Myoplasm Compartment |
| JSR | Junctional Sarcoplasmic Reticulum |
| CSR | Corbular Sarcoplasmic Reticulum |
| NSR | Network Sarcoplasmic Reticulum |
| RyR | Ryanodine Receptor |
| IP ₃ R | Inositol Trisphosphate Receptor |
| V | Membrane Voltage (mV) |
| E _x | Reversal potential of current x (mV) |
| G _x | Maximum conductance of current x (ms/μF) |
| x _∞ | Steady state value of variable x |
| x _τ | Time constant of variable x |
| α _x | Opening rate constant of gate x |
| β _x | Closing rate constant of gate x |
| P _x | Permeability to ion x (cm/s) |
| P _{x,y} | Permeability ratio of ion x to ion y |
| z _x | Valence of ion x |
| v _x | Volume of compartment x |
| R | Gas constant (8314 J/kmol/K) |
| T | Temperature (310K) |
| F | Faraday constant (96487 C/mol) |
| A _{Cap} | Capacitive membrane area (cm ²) |
| A _{Geo} | Geometric membrane area (cm ²) |
| CAMKII | Ca ²⁺ /calmodulin-dependent protein kinase II |
| CAMK _{bound} | Fraction of CAMKII binding sites bound to Ca ²⁺ /calmodulin |
| CAMK _{trap} | Fraction of autonomous CAMKII binding sites with trapped calmodulin |
| CAMK _{active} | Fraction of active CAMKII binding sites |
| CAMK ₀ | Fraction of active CAMKII binding sites at equilibrium |
| α _{CAMK} , β _{CAMK} | Phosphorylation and dephosphorylation rates of CAMKII (ms ⁻¹) |

PLB Phospholamban

Currents, Pumps, Exchangers ($\mu\text{A}/\mu\text{F}$)

| | |
|---------------------|---|
| I_{Na} | Fast Na^+ current |
| I_{NaL} | Slowly inactivating late Na^+ current |
| $I_{\text{NaL},2}$ | Type 2 component of I_{NaL} with its I-V curve peaked at -20mV |
| $I_{\text{NaL},3}$ | Type 3 component of I_{NaL} in the pacemaker range |
| I_{CaL} | Ca^{2+} current through the L-type Ca^{2+} channel |
| I_{CaT} | Ca^{2+} current through the T-type Ca^{2+} channel |
| I_{pCa} | Sarcolemmal Ca^{2+} pump |
| I_{Cab} | Background Ca^{2+} current |
| I_{Kr} | Rapid delayed rectifier K^+ current |
| I_{Ks} | Slow delayed rectifier K^+ current |
| I_{K1} | Inward rectifier K^+ current |
| I_{f} | Hyper-polarization activated Na^+ - K^+ current |
| $I_{\text{f,Na}}$ | Hyper-polarization activated Na^+ current |
| $I_{\text{f,K}}$ | Hyper-polarization activated K^+ current |
| I_{to1} | 4-AP sensitive transient outward K^+ current |
| I_{NaK} | Na^+ - K^+ pump current |
| I_{NCX} | Na^+ - Ca^{2+} exchanger current |
| $I_{\text{Ca,tot}}$ | Total transmembrane Ca^{2+} current $I_{\text{Ca,tot}}=I_{\text{CaL}}+I_{\text{Cab}}+I_{\text{pCa}}+I_{\text{CaT}}-2(I_{\text{NCX,SSL}}+I_{\text{NCX,PCS}})$ |
| $I_{\text{K,tot}}$ | Total transmembrane K^+ current $I_{\text{K,tot}}=I_{\text{Kr}}+I_{\text{Ks}}+I_{\text{K1}}-2I_{\text{NaK}}+I_{\text{to1}}+I_{\text{f,k}}$ |
| $I_{\text{Na,tot}}$ | Total transmembrane Na^+ current $I_{\text{Na,tot}}=I_{\text{Na}}+I_{\text{NaL}}+I_{\text{Nab}}+3I_{\text{NaK}}+I_{\text{f,Na}}+3(I_{\text{NCX,SSL}}+I_{\text{NCX,PCS}})$ |
| I_{tot} | Total transmembrane current $I_{\text{tot}}=I_{\text{Ca,tot}}+I_{\text{K,tot}}+I_{\text{Na,tot}}$ |

Gates

| | |
|---------------------------------|--|
| m,h,j | Activation gate, fast inactivation gate, and slow inactivation gate of I_{Na} , respectively |
| $m_{\text{L2}}, h_{\text{L2}}$ | Activation gate and slow inactivation gate of $I_{\text{NaL},2}$, respectively |
| $m_{\text{L3}}, h_{\text{L3}}$ | Activation gate and slow inactivation gate of $I_{\text{NaL},3}$, respectively |
| d, f, f_2 | Activation gate, fast voltage-dependent inactivation gate, and slow voltage dependent inactivation gate of I_{CaL} , respectively |
| $f_{\text{Ca}}, f_{\text{Ca2}}$ | Fast Ca^{2+} -dependent inactivation gate and slow Ca^{2+} -dependent inactivation gate of I_{CaL} , respectively |
| $X_{\text{1s}}, X_{\text{2s}}$ | Fast activation gate and slow activation gate of I_{Ks} , respectively |
| xr | Activation gate of I_{Kr} |

| | |
|--------------------|--|
| r_{kr} | Time-independent rectification gate of I_{Kr} |
| K_1 | Inactivation gate of I_{K1} |
| a, i, i_2 | Activation gate, fast inactivation gate, and slow inactivation gate of I_{to} , respectively |
| a_{sus}, i_{sus} | Activation gate and inactivation gate of I_{sus} , respectively |
| y | Activation gate of I_f |

Fluxes (mmol /L /ms)

| | |
|---------------|--|
| J_{RyR3} | Ca^{2+} release from RyR3 |
| J_{IP3R} | Ca^{2+} release from IP_3R |
| J_{RyR2} | Ca^{2+} release from RyR2 |
| $J_{tr,j}$ | Ca^{2+} translocation from NSR to JSR |
| $J_{tr,c}$ | Ca^{2+} translocation from NSR to CSR |
| J_{leak} | Ca^{2+} leak from NSR to Myo |
| $J_{leak,s}$ | Ca^{2+} leak from NSR to SSL |
| J_{SERCA} | Ca^{2+} uptake from Myo to NSR via SERCA |
| J_{diff} | Ionic diffusion from PCS to SSL |
| J_{gap} | Ionic diffusion from SSL to Myo |
| τ_{diff} | Time constant for diffusion from PCS to SSL (ms) |
| τ_{gap} | Time constant for diffusion from SSL to Myo (ms) |
| τ_{tr} | Time constant for Ca^{2+} translocation from NSR to JSR/CSR (ms) |

Calcium Buffers

| | |
|---------------|---|
| $CMDN_{Myo}$ | Calmodulin, Ca^{2+} buffer in Myo |
| $TRPN_{Myo}$ | Troponin, Ca^{2+} buffer in Myo |
| $CMDN_{SSL}$ | Calmodulin, Ca^{2+} buffer in SSL |
| $TRPN_{SSL}$ | Troponin, Ca^{2+} buffer in SSL |
| BSR | Anionic SR binding sites for Ca^{2+} buffer in PCS |
| BSL | Anionic sarcolemmal binding sites for Ca^{2+} buffer in PCS |
| β_{PCS} | Buffer factor for PCS |
| $CSQN_{JSR}$ | Calsequestrin, Ca^{2+} buffer in JSR |
| $CSQN_{CSR}$ | Calsequestrin, Ca^{2+} buffer in CSR |

Ionic Concentrations (mmol/L)

| | |
|---------------|--|
| $[Ca^{2+}]_x$ | Ca^{2+} concentration in compartment x, (e.g. $x=i$ indicates the Myoplasmic compartment) |
| $[Na^+]_x$ | Na^+ concentration in compartment x |
| $[K^+]_x$ | K^+ concentration in compartment x |

II MODEL BASIC PARAMETERS

Stimulus

Current stimulus of amplitude $-80.0 \mu A/\mu F$ and duration 0.5 ms is applied during pacing protocols.

External concentrations

$$[Na^+]_o = 140 \text{ mM}; [Ca^{2+}]_o = 1.8 \text{ mM}; [K^+]_o = 5.4 \text{ mM}$$

Initial conditions

| | |
|------------------------------------|--------|
| V | -85.0 |
| m | 0.0 |
| h | 0.9 |
| j | 0.9 |
| d | 0.0 |
| f | 0.9 |
| f2 | 0.9 |
| fca | 0.9 |
| fca2 | 0.9 |
| xs1 | 0.0 |
| xs2 | 0.0 |
| xr | 0.0 |
| a | 0.0 |
| i | 0.9 |
| i2 | 0.9 |
| aa | 0.0 |
| m _{L2} | 0.0 |
| m _{L3} | 0.0 |
| h _{L2} | 0.9 |
| h _{L3} | 0.9 |
| b | 0.0 |
| g | 0.9 |
| u | 0.0 |
| y | 0.0 |
| [Ca ²⁺] _{PCS} | 0.0001 |
| [Ca ²⁺] _{JSR} | 1.0 |
| [Ca ²⁺] _{CSR} | 1.0 |
| [Ca ²⁺] _{NSR} | 1.0 |
| [Ca ²⁺] _{SSL} | 0.0001 |
| [Ca ²⁺] _i | 0.0001 |
| [Na ⁺] _i | 8.0 |
| [K ⁺] _i | 140 |
| [CAMK] _{trap} | 0.0 |

Reversal potentials

$$E_{Na} = \frac{RT}{F} \cdot \ln\left(\frac{[Na^+]_o}{[Na^+]_{SSL}}\right)$$

$$E_K = \frac{RT}{F} \cdot \ln\left(\frac{[K^+]_o}{[K^+]_i}\right)$$

$$E_{Ca} = \frac{RT}{F} \cdot \ln\left(\frac{[Ca^{2+}]_o}{[Ca^{2+}]_{SSL}}\right)$$

III MODEL EQUATIONS AND VALIDATION

Experimental Data Selection Criteria

1. Validation of ionic currents:

Experimental data used to validate the Pcell model were either from un-diseased canine Purkinje fibers or isolated cells at 37 °C. For the validation of individual ionic currents, we preferred experimental studies (Han et al¹) that provided measurements of multiple ionic currents, recorded under the same experimental conditions. Among voltage-clamp studies that provided measurements of the same ionic current (i.e. I_{K1} ^{1,2}), preference was given to those providing additional information that allowed for more rigorous validation, (e.g. dependence on extracellular ionic concentrations). For instance, we validated Pcell I_{K1} current using data from Shah et al², where I-V relationship and $[K^+]_o$ dependence are both available.

2. Validation of ionic concentrations:

Although it is well accepted that intracellular Na content in Pcell is higher than that of Vcell³, there is paucity of experimental data that directly quantify steady-state Na accumulation during pacing at different cycle lengths (CL). Validation of the intracellular Na content is based on experimental measurements of Na ion activity of constantly driven canine cardiac Purkinje fibers⁴. For validation of simulated Pcell Ca dynamics, we used both earlier and more recent experimental data. Early Ca measurements using Aequorin⁵ revealed the biphasic L1-L2 morphology of the Ca^{2+} transient (CaT) and described the dynamic response of L1 and L2 to drug application. Despite the relatively low sensitivity of Aequorin to local Ca, these experiments are well suited for validation of the model subcellular organization of Ca cycling. Importantly, recent data from confocal microscopic studies⁶ using fluorescence imaging were used for the validation of other CaT properties, including diastolic concentration, magnitude during the AP and time course of relaxation.

3. Validation of the Action Potential (AP):

3.1 AP Morphology:

Even under similar experimental conditions, morphology of AP recorded from isolated canine Purkinje cells demonstrates large differences (probably related to the isolation procedure¹). With these differences, canine Purkinje AP morphology can be characterized by the following consistent properties: fast upstroke (dV/dt_{max} of about 500 v/s; faster than Vcell), sloping repolarization time course during phase-2, slower repolarization during phase-3 compared to Vcell, and similar resting potential to that of Vcell. The Pcell model formulated here reproduces these characteristics that are distinct and typical to Purkinje AP (Figure 2A, main text).

3.2 AP rate dependence:

Most experimental data of Purkinje AP rate dependence are based on measurements in Purkinje fibers. While more consistent than single-cell recordings, results still vary. For example, steady-state measurements of APD in isolated canine Purkinje fibers at CL=2000ms range from 350ms to 450ms^{7,8}. Such variation (100ms) in APD is much larger than the differences between fiber and single cell measurements due to electrotonic influences (10ms⁹). Thus, the more consistent experimental measurements in Purkinje fibers were used to validate the simulated Purkinje AP rate dependence (Figure 2B, main text).

Fast Sodium Current (I_{Na})

Formulation of I_{Na} is modified from the Hund-Decker-Rudy (HRd) model⁹ to achieve maximum upstroke velocity (dV/dt_{max}) and amplitude of Purkinje AP that are consistent with experimental measurements⁷.

Equations:

$$\alpha_m = \frac{0.64 \cdot (V + 37.13)}{1 - e^{-0.1 \cdot (V + 37.13)}}$$

$$\beta_m = 0.16 \cdot e^{-\left(\frac{V}{11}\right)}$$

If $V \geq -40.0mV$

$$\alpha_h = 0.0$$

$$\beta_h = \frac{1}{0.13 \cdot (1 + e^{-\left(\frac{V+10.66}{11.1}\right)})}$$

$$\alpha_j = 0.0$$

$$\beta_j = \frac{0.6 \cdot e^{-2.535 \times 10^{-7} \cdot V}}{1 + e^{-\left(\frac{V+32}{10}\right)}}$$

else

$$\alpha_h = 0.135 \cdot e^{-\left(\frac{V+70}{6.8}\right)}$$

$$\beta_h = 3.56 \cdot e^{0.079 \cdot V} + 3.1 \times 10^5 \cdot e^{0.35 \cdot V}$$

$$\alpha_j = \frac{(-2.5428 \times 10^5 \cdot e^{0.2444 \cdot V} - 13.896 \times 10^5 \cdot e^{-0.04391 \cdot V}) \cdot (V + 37.78)}{1 + e^{0.311 \cdot (V_m + 79.23)}}$$

$$\beta_j = \frac{0.2424 \cdot e^{-0.01052 \cdot V}}{1 + e^{-0.1378 \cdot (V + 40.14)}}$$

$$\bar{G}_{Na} = 18 \text{ mS}/\mu\text{F}$$

$$I_{Na} = \bar{G}_{Na} \cdot m^3 \cdot h \cdot j \cdot (V - E_{Na})$$

Late Sodium Current (I_{NaL})

Two populations of I_{NaL} ($I_{NaL,2}$ and $I_{NaL,3}$) are included in the model, based on canine purkinje data from Vassalle and coworkers^{10,11}. It was shown using voltage clamp that $I_{NaL,2}$ activated at -50mV and reached its peak at -20mV. Time constant for activation of I_{NaL} is the same as that of I_{Na} . $I_{NaL,2}$ voltage dependence of activation, inactivation and the time constant for inactivation were fitted to the data of Vassalle et al¹⁰ (Figure S1). The $I_{NaL,2}$ I-V curve is in agreement with experimental recordings (Figure S1 A). Compared to $I_{NaL,2}$, $I_{NaL,3}$ is characterized by smaller current density, faster inactivation and left-shifted voltage-dependent activation (35mV)¹¹.

Equations:

$$m_{L2,\tau} = \frac{1}{\frac{0.64 \cdot (V + 37.13)}{1 - e^{-0.1 \cdot (V + 37.13)}} + 0.16 \cdot e^{-\left(\frac{V}{11}\right)}}$$

$$m_{L2,\infty} = \frac{1}{1 + e^{-\frac{(V+28)}{7}}}$$

$$m_{L3,\tau} = m_{L2,\tau}$$

$$m_{L3,\infty} = \frac{1}{1 + e^{-\frac{(V+63)}{7}}}$$

$$h_{L2,\tau} = 162 + \frac{132}{1 + e^{-\frac{V+28}{5.5}}}$$

$$h_{L2,\infty} = \frac{1}{1 + e^{-\frac{(V+28)}{12}}}$$

$$h_{L3,\tau} = 0.5 \cdot h_{L2,\tau}$$

$$h_{L3,\infty} = \frac{1}{1 + e^{-\frac{(V+63)}{12}}}$$

$$j_{L2,\tau} = 411$$

$$j_{L2,\infty} = m_{L2,\infty}$$

$$j_{L3,\tau} = 0.5 \cdot j_{L2,\tau}$$

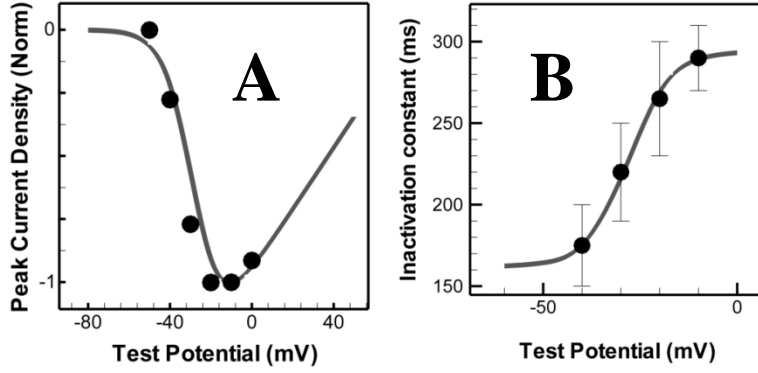
$$j_{L3,\infty} = m_{L3,\infty}$$

$$\bar{G}_{NaL,2} = 0.052 \text{ mS}/\mu\text{F}; \bar{G}_{NaL,3} = 0.018 \text{ mS}/\mu\text{F}$$

$$I_{NaL,2} = \bar{G}_{NaL,2} \cdot m_{L2} \cdot h_{L2} \cdot j_{L2} \cdot (V - E_{Na})$$

$$I_{NaL,3} = \bar{G}_{NaL,3} \cdot m_{L3} \cdot h_{L3} \cdot j_{L3} \cdot (V - E_{Na})$$

$$I_{NaL} = I_{NaL,2} + I_{NaL,3}$$



Online Figure I. $I_{NaL,2}$ Model Validation. Experimental data are from Vassalle et al¹⁰ (dots). Simulation results are shown as solid gray lines. (A) I-V curve (B) Inactivation time constant.

L-type Calcium Current (I_{CaL})

I_{CaL} is a smaller current in canine Purkinje cells compared to ventricular myocytes. Steady state activation and inactivation, and fast and slow inactivation time constants are fitted using data from canine purkinje cells published by Han et al¹ (Figure S2). I-V curve of I_{CaL} is in agreement with experimental measurements (Figure S2 C). Calcium dependent inactivation and CAMKII dependence of I_{CaL} are the same as in HRd model.

Equations:

$$d_{\infty} = \frac{1}{1 + e^{-\frac{(V-2)}{7.8}}}$$

$$d_{\tau} = 0.59 + 0.8 \cdot \frac{e^{0.052 \cdot (V+13)}}{1 + e^{0.132 \cdot (V+13)}}$$

$$f_{\infty} = \frac{1}{1 + e^{\frac{V+16.5}{9.5}}}$$

$$f_{\tau} = \frac{1}{0.1358696 \cdot e^{-0.00261 \cdot (V-2.5)^2} + 0.10869565}$$

$$f_{2,\infty} = f_{\infty}$$

$$f_{2,\tau} = \frac{1}{0.2222222 \cdot e^{-0.0018 \cdot (V-18.6)^2} + 0.00555555}$$

$$f_{Ca,\infty} = \frac{0.3}{1 - \frac{I_{CaL}}{0.05}} + \frac{0.55}{1 + \frac{[Ca^{2+}]_{PCS}}{0.003}} + 0.15$$

$$f_{Ca,\tau} = \frac{10}{1 + \frac{K_{mCAM}}{CAMK_{active}}} + 0.5 + \frac{1}{1 + \frac{[Ca^{2+}]_{PCS}}{0.003}}$$

$$f_{Ca,2,\infty} = \frac{300}{1 + e^{-\frac{0.175 + I_{CaL}}{0.04}}} + 125$$

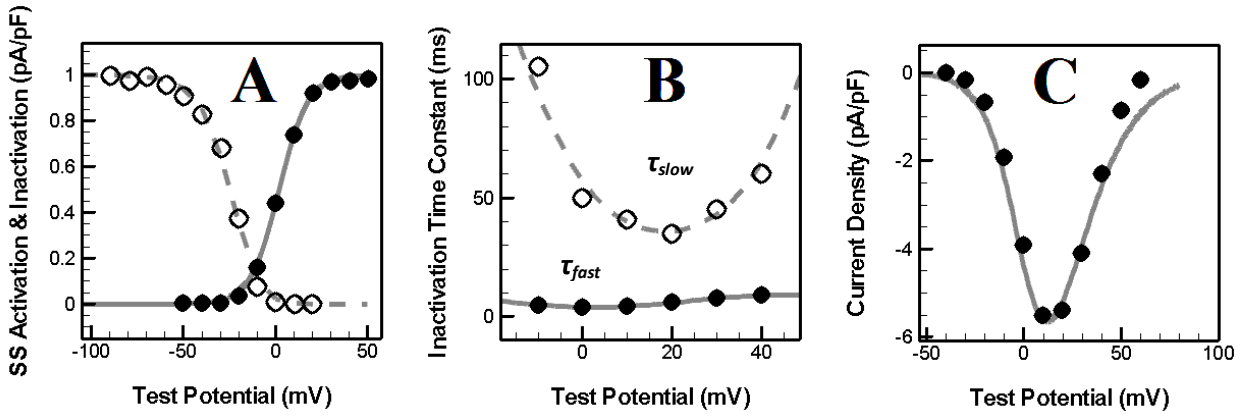
$$P_{Ca} = 1.9926 \times 10^{-4} \text{ cm/s}$$

$$\gamma_{cai} = 1$$

$$\gamma_{cao} = 0.341$$

$$\bar{I}_{CaL} = P_{Ca} \cdot z_{Ca}^2 \cdot \frac{V \cdot F^2}{RT} \cdot \frac{\gamma_{cai} \cdot [Ca^{2+}]_{PCS} \cdot e^{\frac{z_{Ca} \cdot V \cdot F}{RT}} - \gamma_{cao} \cdot [Ca^{2+}]_o}{e^{\frac{z_{Ca} \cdot V \cdot F}{RT}} - 1}$$

$$I_{CaL} = \bar{I}_{CaL} \cdot d \cdot f \cdot f_2 \cdot f_{ca} \cdot f_{ca,2}$$



Online Figure II. I_{CaL} Model Validation. Experimental data are from Han et al¹ (dots). Simulation results are shown as gray lines. (A) voltage dependence of steady state activation and inactivation. (B) slow and fast inactivation time constants. (C) I-V curve.

T-type Calcium Current (I_{CaT})

I_{CaT} is a larger current in canine Purkinje cells compared to ventricular myocytes. Steady state activation and inactivation are fitted using canine Purkinje cell data from Han et al¹ (Figure S3 A). I-V curve of I_{CaT} is in agreement with experimental measurements (Figure S3 B). It should be noted that the T/L ratio (the ratio between maximum T type and L type Ca current densities) measured by Han et al¹ and computed in the model is 0.8. This ratio is larger than earlier reported values (0.6) (Hirano et al¹², Tseng and Boyden¹³). The difference could be accounted for by differences between voltage clamp protocols (in holding potential and $[Ca^{2+}]_o$). However, this difference has minimal effect on the Pcell AP (reduction of T/L ratio to 0.6 in the model does not change AP morphology and shortens APD by only 1ms). We chose Han et al¹ data for I_{CaT} validation because this publication provides data for several other currents, recorded under the same experimental conditions.

Equations:

$$b_{\infty} = \frac{1}{1 + e^{\frac{-(V-30)}{7}}}$$

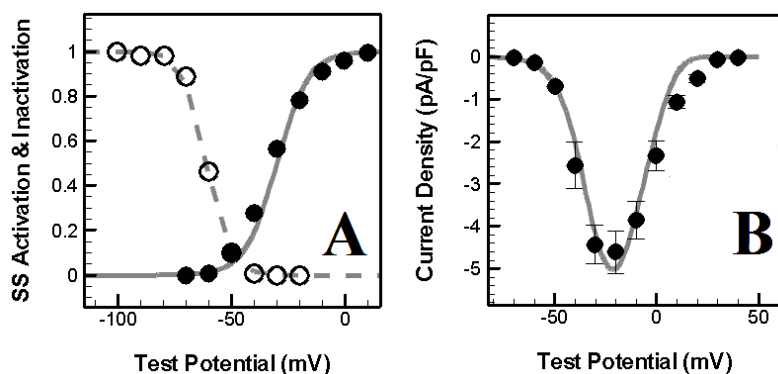
$$b_{\tau} = \frac{1}{1.068 \cdot e^{\frac{V+16.3}{30}} + 1.068 \cdot e^{\frac{V+16.3}{30}}}$$

$$g_{\infty} = \frac{1}{1 + e^{\frac{(V+61)}{5}}}$$

$$b_{\tau} = \frac{1}{0.015 \cdot e^{\frac{V+71.7}{83.3}} + 0.015 \cdot e^{\frac{V+71.7}{15.4}}}$$

$$\bar{G}_{CaT} = 0.07875 \text{ mS}/\mu\text{F}$$

$$I_{CaT} = \bar{G}_{CaT} \cdot b \cdot g \cdot (V - E_{Ca})$$



Online Figure III. I_{CaT} Model Validation. Experimental data are from Han et al¹ (dots). Simulation results are shown as gray lines. (A) steady state voltage dependence of steady-state activation and inactivation. (B)

I-V curve.

Transient Outward Potassium Current (I_{to1})

Formulation of I_{to1} is fitted to canine Purkinje cell data from Han et al¹ and Dumaine and Cordeiro¹⁴ (Figure S4). I_{to1} consists of a transient outward current with slow time-dependent recovery (I_{to}) and an instantaneous sustained current (I_{sus}).

I_{to} is more rate dependent in Purkinje cells than in ventricular myocytes¹⁵. Voltage dependent activation and inactivation, slow and fast inactivation time constants and I-V curve are in agreement with experimental measurements¹ (Figure S4 A-C). Simulated I_{to} reactivation time course (Figure S4 D) is in agreement with experimental data from Han et al¹.

The formulation of I_{sus} is modified from previous modeling studies^{16,17}, assuming instantaneous activation. This is consistent with experimental recordings that show no rate dependence of this current (Jeck et al¹⁸ and Han et al¹⁵). The simulated I-V curve is in agreement with experimental measurements by Dumaine and Cordeiro¹⁴ (Figure S4 E).

Equations:

$$a_{\tau} = \frac{1}{\frac{25 \cdot e^{\frac{V-82}{18}}}{1 + e^{\frac{V-82}{18}}} + \frac{25 \cdot e^{\frac{V+52}{18}}}{1 + e^{\frac{V+82}{18}}}}$$

$$i_{\tau} = \frac{1}{0.1 \cdot e^{\frac{V+125}{15}} + 0.1 \cdot e^{\frac{V+2}{26.5}}} + 2.86$$

$$i_{2,\tau} = \frac{1}{0.005 \cdot e^{\frac{V+138.2}{52}} + 0.003 \cdot e^{\frac{V+18}{12.5}}} + 21.5$$

$$a_{\infty} = \frac{1}{1 + e^{\frac{-(V-8.9)}{10}}}$$

$$i_{\infty} = \frac{1}{1 + e^{\frac{V+32}{11.2}}}$$

$$i_{2,\infty} = i_{\infty}$$

$$a_{sus} = \frac{1}{1 + e^{\frac{-(V-3.0)}{19.8}}}$$

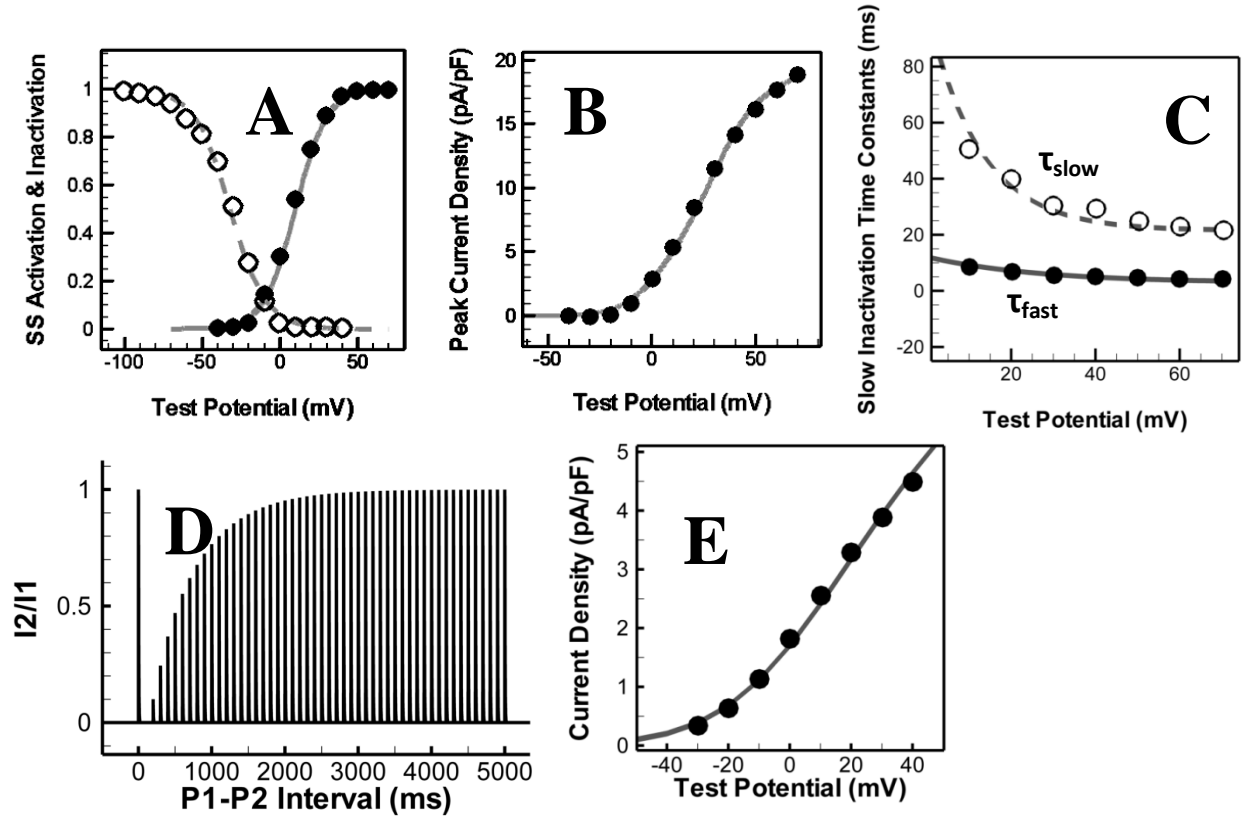
$$\bar{G}_{to} = 0.1414 \text{ mS}/\mu\text{F}$$

$$\bar{G}_{sus} = 0.042 \text{ mS}/\mu\text{F}$$

$$I_{to,s} = \bar{G}_{to} \cdot a \cdot i \cdot i_2 \cdot (V - E_K)$$

$$I_{to,f} = \bar{G}_{sus} \cdot a_{sus} \cdot (V - E_K)$$

$$I_{to1} = I_{to} + I_{sus}$$



Online Figure IV. I_{to} and I_{sus} Model Validation. Experimental data are from Han et al¹ (I_{to}) and Dumaine and Cordeiro¹⁴ (I_{sus}) (dots). Simulation results are shown as gray lines. (A) voltage dependence of steady-state activation and inactivation. (B) I-V curve. (C) fast (solid) and slow (dashed) inactivation time constants. (D) Simulated I_{to} reactivation time course obtained from a double-pulse (P1-P2) protocol. (E) I_{sus} I-V curve.

Slow Delayed Rectifier Potassium Current (I_{Ks})

Formulation of I_{Ks} is fitted to canine Purkinje cell data from Han et al¹ (Figure S5). Slow and fast activation time constants, and I-V relationship are in agreement with experimental measurements.

Equations:

$$E_{Ks} = \frac{RT}{F} \cdot \ln\left(\frac{[K^+]_o + P_{Na,K} \cdot [Na^+]_o}{[K^+]_i + P_{Na,K} \cdot [Na^+]_{SSL}}\right)$$

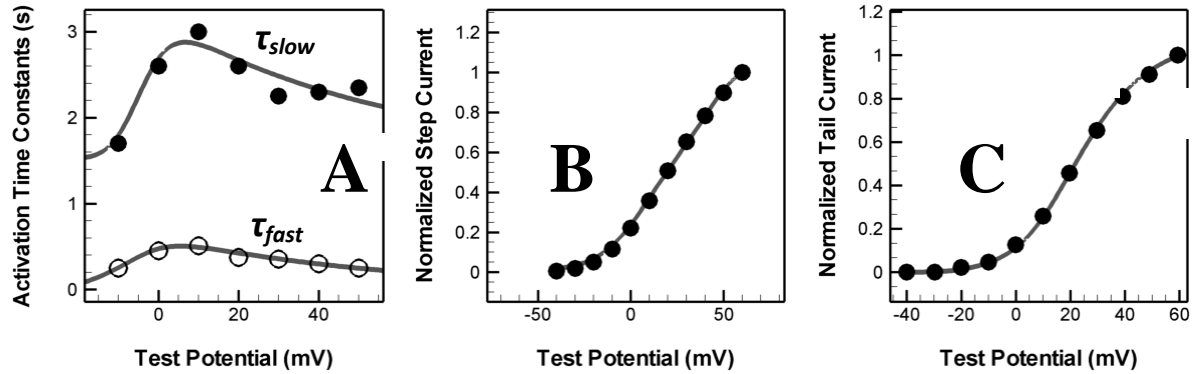
$$\bar{G}_{Ks} = 0.053 \cdot \left(1 + \frac{0.6}{1 + \left(\frac{3.8 \times 10^{-5}}{[Ca^{2+}]_{SSL}}\right)^{1.4}}\right)$$

$$X_{1s,\infty} = X_{2s,\infty} = \frac{1}{1 + e^{-\frac{V-10.5}{24.7}}}$$

$$X_{1s,\tau} = \frac{200}{e^{-\frac{V+10}{6}} + e^{\frac{V-62}{55}}}$$

$$X_{2s,\tau} = 1500 + \frac{350}{e^{-\frac{V+10}{4}} + e^{\frac{V-90}{58}}}$$

$$I_{Ks} = \bar{G}_{Ks} \cdot X_{1s} \cdot X_{2s} \cdot (V - E_{Ks})$$



Online Figure V. I_{Ks} Model Validation. Experimental data are from Han et al¹ (dots). Simulation results are shown as gray lines. (A) slow and fast activation time constants. (B), (C) I-V curves for step and tail currents, respectively.

Slow Delayed Rectifier Potassium Current (I_{Kr})

Formulation of I_{Kr} is fitted to canine Purkinje cell data from Han et al¹ (Figure S6). Simulated I-V curve is in agreement with experimental measurements¹ (Figure S6).

Equations:

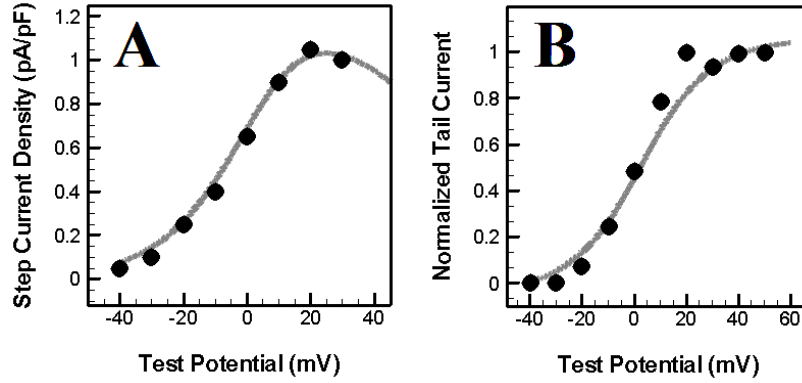
$$xr_{\infty} = \frac{1}{1 + e^{-\frac{V}{15}}}$$

$$xr_{\tau} = 100 + \frac{400}{1 + e^{\frac{V}{10}}}$$

$$rkr = \frac{1}{1 + e^{\frac{V}{35}}}$$

$$\bar{G}_{Kr} = 0.03262 \cdot \sqrt{\frac{[K^+]_o}{5.4}}$$

$$I_{Kr} = \bar{G}_{Kr} \cdot xr \cdot rkr \cdot (V - E_K)$$



Online Figure VI. I_{Kr} Model Validation. Experimental data are from Han et al¹ (dots). Simulation results are shown as gray lines. I-V curves for step current (A) and tail current (B).

Hyper-polarization Activated Current (I_f)

Formulation of I_f is modified from Maltsev and Lakatta¹⁷. I_f is carried by HCN (Hyperpolarization-activated, cyclic nucleotide-gated) channels¹⁹. Steady state activation is adjusted to fit experimental data for HCN2 channels¹⁹, reflecting the high expression level of HCN2 in canine Purkinje cells²⁰. The time constant for activation and the current density are fitted to canine Purkinje data from Yu et al²¹.

Equations:

$$y_{\infty} = \frac{1}{1 + e^{-\frac{V+87}{9.5}}}$$

$$y_{\tau} = \frac{2000}{e^{-\frac{V+132}{10}} + e^{-\frac{V+57}{60}}}$$

$$I_{fNa} = 0.012 \cdot y^2 \cdot (V - E_{Na})$$

$$I_{fK} = 0.024 \cdot y^2 \cdot (V - E_K)$$

$$I_f = I_{fNa} + I_{fK}$$

Time-independent inward rectifier potassium current (I_{K1})

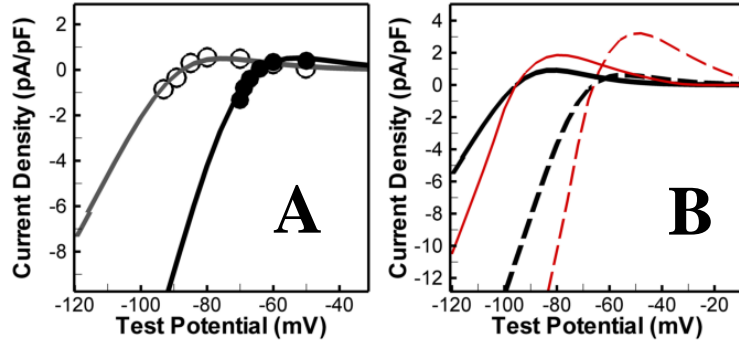
Formulation of I_{K1} is modified from the HRd model. I-V curve and its dependence on $[K^+]_o$ are fitted to experimental data from Shah et al², where I_{K1} was measured as 10mM Cs^+ sensitive current (Figure S7).

Equations:

$$K_1 = \frac{1}{1 + e^{-\frac{V+100.1-2.175 \cdot [K^+]_o}{10.15}}}$$

$$\bar{G}_{K1} = 0.12 \cdot \sqrt{[K^+]_o}$$

$$I_{K1} = \bar{G}_{K1} \cdot K_1 \cdot (V - E_K)$$



Online Figure VII. I_{K1} Model Validation. (A) Experimental data are from Shah et al² ($[K^+]_o = 4\text{mM}$ (open circles) and 12mM (filled circles)). Simulation results are shown as gray ($[K^+]_o = 4\text{mM}$) and black ($[K^+]_o = 12\text{mM}$) lines. (B) Comparison of simulated I_{K1} $[K^+]_o$ dependence in canine Purkinje (Black) and Ventricular (Red) cells; $[K^+]_o = 4\text{mM}$ (solid) and $[K^+]_o = 12\text{mM}$ (dashed).

Sodium-Calcium Exchanger (I_{NCX})

Formulation of I_{NCX} is the same as in the HRd model, with a reduced current density based on reduced expression level of $\text{Na}^+ \text{-Ca}^{2+}$ exchanger protein (NCX1) in canine Purkinje cells compared to ventricular myocytes²⁰.

Equations:

$$v_{max} = 2.925 \mu\text{A}/\mu\text{F}; k_{sat} = 0.27; \eta = 0.35$$

$$K_{m,Nai} = 12.3 \text{ mM}/L; K_{m,NaO} = 87.5 \text{ mM}/L;$$

$$K_{m,Cai} = 0.0036 \text{ mM}/L; K_{m,CaO} = 1.3 \text{ mM}/L;$$

$$K_{mCa,act} = 1.25 \times 10^{-4} \text{ mM}/L;$$

$$I_{NaCa_x} = Allo_x \cdot \Delta E_x$$

$$Allo_x = \frac{1}{1 + \left(\frac{K_{mCa,act}}{1.5 \cdot [Ca^{2+}]_x}\right)^2}$$

$$\Delta E_x$$

$$= \frac{v_{max} \cdot ([Na^+]_i^3 \cdot [Ca^{2+}]_o \cdot e^{\eta \frac{VF}{RT}} - [Na^+]_i^3 \cdot 1.5 \cdot [Ca^{2+}]_x \cdot e^{(\eta-1) \frac{VF}{RT}})}{\left(1 + k_{sat} \cdot e^{\frac{(\eta-1) \cdot VF}{RT}}\right) \cdot (K_{m,CaO} \cdot [Na^+]_i^3 + K_{m,NaO}^3 \cdot 1.5 \cdot [Ca^{2+}]_x + K_{m,Nai}^3 \cdot [Ca^{2+}]_o \cdot \left(1 + \frac{1.5 \cdot [Ca^{2+}]_x}{K_{m,Cai}}\right)) + K_{m,Cai} \cdot [Na^+]_o^3 \cdot \left(1 + \frac{[Na^+]_i^3}{K_{m,Nai}^3}\right) + [Na^+]_i^3 \cdot [Ca^{2+}]_o + [Na^+]_o^3 \cdot 1.5 \cdot [Ca^{2+}]_i}$$

$$I_{NaCa} = 0.8 \cdot I_{NaCa_{SSL}} + 0.2 \cdot I_{NaCa_{PCS}}$$

Sodium-Potassium Pump (I_{NaK})

Formulation of I_{NaK} is modified from the HRd model. Half saturation coefficient for extracellular potassium is adjusted to 0.8 mM, as suggested by Cohen et al²². Gao et al²³ reported identical dependence of I_{NaK} on both voltage and intracellular sodium in canine Epi- and Endo- myocardium. Here, we assume similar dependence for Purkinje I_{NaK} . Current density of I_{NaK} is reduced based on reduced expression level of Na^+/K^+ ATPase in Purkinje cells compared to ventricular myocytes²⁴ (human data). We assume that the relative difference between expression levels of Na^+/K^+ ATPase in human Purkinje and ventricular cells is similar in canine²⁵. With intracellular sodium of 10mM and resting membrane potential at -78 mV, simulated resting Na/K pump current is 0.3 pA/pF, which is within the range of experimental measurements (0.27 pA/pF (Cohen et al²²); 0.6 pA/pF (Boyden et al²⁶)). Differences in experimental measurements are likely due to different intracellular Na and resting membrane potential.

Equations:

$$\bar{I}_{NaK} = 1.1004 \mu A/\mu F$$

$$f_v = \frac{1}{1 + e^{-\frac{(V+92) \cdot F}{R \cdot T}}}$$

$$P_{Na} = \left(\frac{[Na^+]_{SSL}}{[Na^+]_{SSL} + 2.6} \right)^3$$

$$P_K = \frac{[K^+]_o}{[K^+]_o + 0.8}$$

$$I_{NaK} = \bar{I}_{NaK} \cdot f_v \cdot P_{Na} \cdot P_K$$

Sarcolemmal Calcium Pump (I_{pCa}), Background Calcium Current (I_{Cab}) and Background Sodium Current (I_{Nab})

Formulations of these two currents are the same as in the HRd model, with adjusted current amplitudes.

Equations:

$$\bar{G}_{pCa} = 0.0115 mS/\mu F$$

$$K_{m,pCa} = 0.0005 mM$$

$$I_{pCa} = \frac{\bar{G}_{pCa}}{1 + \frac{K_{m,pCa}}{[Ca^{2+}]_{SSL}}}$$

$$P_{Cab} = 3.99 \times 10^{-8} cm/s; \gamma_{Cai} = 1; \gamma_{Cao} = 0.341$$

$$I_{Cab} = P_{Cab} \cdot z_{Ca}^2 \cdot \frac{V \cdot F^2}{RT} \cdot \frac{\gamma_{Cai} \cdot [Ca^{2+}]_{SSL} \cdot e^{\frac{z_{Ca} V F}{RT}} - \gamma_{Cao} \cdot [Ca^{2+}]_o}{e^{\frac{z_{Ca} V F}{RT}} - 1}$$

$$P_{Nab} = 0.64 \times 10^{-8} cm/s$$

$$I_{Nab} = P_{Nab} \cdot \frac{V \cdot F^2}{RT} \cdot \frac{[Na^+]_{SSL} \cdot e^{\frac{VF}{RT}} - [Na^+]_o}{e^{\frac{VF}{RT}} - 1}$$

SR Ca²⁺ Fluxes

Formulation for Ca²⁺ release via RyR (RyR3 and RyR2) is modified from Livshitz and Rudy²⁷. Localization of RyR2 and RyR3 is according to their spatial distribution in canine Purkinje cells²⁸. RyR3 responds to Ca²⁺ fluxes in the PCS, including I_{CaL} , J_{RyR3} , J_{IP3R} and J_{diff} ; while RyR2 responds to Ca²⁺ fluxes in Myo, including J_{SERCA} , J_{leak} , J_{gap} and J_{RyR2} . τ_{RyR} and RyR_{∞} are fitted to experimental data^{5,6}, to reproduce accurate morphology, decay and amplitude of the Ca transient ($[Ca^{2+}]_{avg}$) during steady-state pacing at 1Hz.

For validation of simulated Pcell Ca dynamics, we used both earlier and more recent experimental data. Early Ca measurements using Aequorin⁵ revealed the biphasic L1-L2 morphology of CaT and described the dynamic response of L1 and L2 to application of drugs. These experiments are well suited for validation of the Pcell model subcellular organization of Ca²⁺ cycling. Recent confocal microscopic studies using fluorescence imaging⁶ were used for the validation of other CaT properties, including diastolic concentration, magnitude during the AP and time course of relaxation.

During pacing at CL=1000ms, regions of interest (ROI) of canine Purkinje cell aggregate (Boyden et al⁶) showed an increase of fluorescent signal intensity from 30 units to 90 units (assuming that each ROI represents equal portion of the cell aggregate). The 60 units difference can be calibrated to represent an increase of free Ca²⁺ by 260 nM/L. With $[Ca^{2+}]_o$ of 2mM at CL=1000ms, simulated resting and peak levels of $[Ca^{2+}]_{avg}$ are 70nM/L and 310nM/L, respectively. This amounts to an increase of free Ca²⁺ by 240nM/L. Thus, the simulated amplitude of CaT during pacing at CL=1000ms is in agreement with experimental data. Simulated rate dependence curve of CaT (slope = 0.485 with linear fitting) is consistent with measurements of rate dependence of intracellular Ca activity (slope = 0.5 with linear fitting) recorded from sheep Purkinje strand (Lado et al²⁹).

Average time of CaT half decay (τ) measured by fluorescent signal, is ~150ms (Boyden et al⁶) during pacing at CL=1000ms. Simulated τ of $[Ca^{2+}]_{avg}$ during steady-state pacing at CL=1000ms is 156ms, consistent with experiments. The simulated L1 component of peak CaT occurs 25ms after the stimulus, while the L2 component occurs after 85ms. This is in good agreement with experimental measurements (30ms for L1 and 80ms for L2; Hess et al⁵). Value of τ_{diff} is the same as for diffusion between subspace and myoplasm in the HRd model⁹. For $\tau_{gap} = 12ms$, the simulated delay between the L1 and L2 components of CaT is consistent with the delay measured experimentally⁵.

CAMKII regulation of Ca²⁺ release via RyR is the same as in the HRd model⁹.

Equations:

○ RyR3 Ca²⁺ Release:

$$Rel_{RyR3} = -(I_{CaL} \cdot \frac{A_{Cap}}{V_{PCS} \cdot 2 \cdot F} - (J_{RyR3} + J_{IP3R}) \frac{V_{JSR}}{V_{PCS}} + J_{diff})$$

$$\tau_{RyR3} = \frac{2 \cdot (1 + \frac{1}{0.28})}{1 + ([CAMK]_{active})^8}$$

$$1 + \frac{0.0123}{[Ca^{2+}]_{JSR}}$$

if ($Rel_{RyR_3} > 0$)

$$RyR_{3\infty} = \frac{15 \cdot Rel_{RyR_3} \cdot \left(1 + \frac{1}{1 + \left(\frac{0.28}{[CAMK]_{active}}\right)^8}\right)}{1 + \left(\frac{1}{[Ca^{2+}]_{JSR}}\right)^8}$$

else

$$RyR_{3\infty} = 0$$

$$\frac{dJ_{RyR_3}}{dt} = \frac{RyR_{3\infty} - J_{RyR_3}}{\tau_{RyR_3}}$$

○ RyR2 Ca²⁺ Release:

$$Rel_{RyR_2} = -J_{SERCA} \frac{V_{NSR}}{V_{Myo}} + J_{leak} \frac{V_{NSR}}{V_{Myo}} + J_{gap} \frac{V_{SSL}}{V_{Myo}} + J_{RyR_2} \frac{V_{CSR}}{V_{Myo}}$$

$$\tau_{RyR_2} = \frac{6 \cdot \left(1 + \frac{1}{1 + \left(\frac{0.28}{[CAMK]_{active}}\right)^8}\right)}{1 + \frac{0.0123}{[Ca^{2+}]_{CSR}}}$$

if ($Rel_{RyR_2} > 0$)

$$RyR_{2\infty} = \frac{91 \cdot Rel_{RyR_2} \cdot \left(1 + \frac{1}{1 + \left(\frac{0.28}{[CAMK]_{active}}\right)^8}\right)}{1 + \left(\frac{1}{[Ca^{2+}]_{CSR}}\right)^8}$$

else

$$RyR_{2\infty} = 0$$

$$\frac{dJ_{RyR_2}}{dt} = \frac{RyR_{2\infty} - J_{RyR_2}}{\tau_{RyR_2}}$$

○ IP₃R Ca²⁺ Release:

Formulation for Ca²⁺ release via IP₃R is based on Bugrim and Zhabotinsky³⁰ (a simplification of the DeYong and Keizer model³¹). The model of IP₃R considers a ligand binding site for IP₃ and two ligand binding sites for Ca²⁺ (activating and inactivating), and assumes that the rate constants of binding and dissociation of the ligands do not depend on the state of the receptor³⁰. IP₃R is co-localized with RyR3 in the PCS, and both its activation and inactivation depend on the local Ca²⁺ concentration ($[Ca^{2+}]_{PCS}$) and Ca²⁺ in the JSR ($[Ca^{2+}]_{JSR}$) for a fixed level of $[IP_3]$.

$$k_0 = 96000 \text{ mM}^{-1}\text{s}^{-1}; k_{0a} = 9.6\text{s}^{-1}; k_1 = 150000\text{mM}^{-1}\text{s}^{-1}; k_{1a} = 16.5\text{s}^{-1};$$

$$k_2 = 1800\text{mM}^{-1}\text{s}^{-1}; k_{2a} = 0.21\text{s}^{-1}; \tau_{IP_3R} = 3.7\text{s}^{-1};$$

$$[IP_3] = 0.001\text{mM/L};$$

$$\frac{du_{IP_3R}}{dt} = [Ca^{2+}]_{PCS} \cdot k_2 \cdot (1 - u_{IP_3R}) - k_{2a} \cdot u_{IP_3R}$$

$$J_{IP_3R} = 10.92 \cdot \frac{\tau_{IP_3R} \cdot [IP_3] \cdot [Ca^{2+}]_{PCS} \cdot (1 - u_{IP_3R})}{\left(1 + \frac{[IP_3] \cdot k_0}{k_{0a}}\right) \cdot \left(1 + [Ca^{2+}]_{PCS} \frac{k_1}{k_{1a}}\right)} ([Ca^{2+}]_{JSR} - [Ca^{2+}]_{PCS})$$

○ **Ca²⁺ Uptake via SERCA:**

Formulation for SR Ca²⁺ ATPase (J_{SERCA}) is modified from the HRd model. Maximum uptake via J_{SERCA} (\bar{J}_{SERCA}) is reduced based on the reduced expression of SERCA2 in Purkinje cells compared to ventricular myocytes²⁰. A small population of J_{SERCA} ($J_{SERCA,s}$) is located in the SSL.

$$\Delta \bar{K}_{m,PLB} = 0.00017mM/L; \Delta \bar{J}_{SERCA,PLB} = 0.75; K_{m,CAMK} = 0.15$$

$$\bar{J}_{SERCA} = 0.0026mM/L \text{ per ms}; \bar{J}_{SERCA,s} = 0.0002mM/L \text{ per ms}; K_{m,SERCA} = 0.00028mM/L$$

$$NSR = 15 \text{ mM/L}$$

$$\Delta K_{m,PLB} = \Delta \bar{K}_{m,PLB} \cdot \frac{CAMK_{active}}{K_{m,CAMK} + CAMK_{active}}$$

$$\Delta J_{SERCA,CAMK} = \Delta \bar{J}_{SERCA,CAMK} \cdot \frac{CAMK_{active}}{K_{m,CAMK} + CAMK_{active}}$$

$$J_{SERCA} = \bar{J}_{SERCA} \cdot \frac{(1 + \Delta J_{SERCA,CAMK})}{1 + \frac{K_{m,SERCA} - \Delta K_{m,PLB}}{[Ca^{2+}]_i}} - 0.0035 \cdot \frac{[Ca^{2+}]_{NSR}}{NSR}$$

$$J_{SERCA,s} = \bar{J}_{SERCA,s} \cdot \frac{(1 + \Delta J_{SERCA,CAMK})}{1 + \frac{K_{m,SERCA} - \Delta K_{m,PLB}}{[Ca^{2+}]_{SSL}}} - 0.000875 \cdot \frac{[Ca^{2+}]_{NSR}}{NSR}$$

○ **Ca²⁺ Translocation Fluxes:**

Formulation of Ca²⁺ translocation fluxes (from NSR to CSR and JSR) is from the HRd model⁹.

$$\tau_{tr} = 120ms$$

$$J_{tr,j} = \frac{([Ca^{2+}]_{NSR} - [Ca^{2+}]_{JSR})}{\tau_{tr}}$$

$$J_{tr,c} = \frac{([Ca^{2+}]_{NSR} - [Ca^{2+}]_{CSR})}{\tau_{tr}}$$

Ionic Concentrations

$$\tau_{diff} = 0.2 \text{ ms}; \tau_{gap} = 12ms$$

$$J_{diff} = \frac{[Ca^{2+}]_{PCS} - [Ca^{2+}]_{SSL}}{\tau_{diff}}$$

$$J_{gap} = \frac{[Ca^{2+}]_{SSL} - [Ca^{2+}]_i}{\tau_{gap}}$$

○ **[Ca²⁺]_{PCS}:**

$$\beta_{PCS} = \frac{1}{1 + \overline{BSR} \cdot \frac{K_{m,BSR}}{([Ca^{2+}]_{PCS} + K_{m,BSR})^2} + \overline{BSR} \cdot \frac{K_{m,BSL}}{([Ca^{2+}]_{PCS} + K_{m,BSL})^2}}$$

$$\frac{d[Ca^{2+}]_{PCS}}{dt} = \beta_{PCS} \cdot (-I_{CaL} - 2 \cdot I_{NaCa,PCS}) \cdot \frac{A_{Cap}}{V_{PCS} \cdot 2 \cdot F} + (J_{RyR_2} + J_{IP_3R}) \cdot \frac{V_{JSR}}{V_{PCS}} - J_{diff}$$

○ $[Ca^{2+}]_{SSL}$:

$$\frac{d[Ca^{2+}]_{SSL}}{dt} = -(I_{CaT} + I_{pCa} + I_{CaB} - 2 \cdot I_{NaCa,SSL}) \cdot \frac{A_{Cap}}{V_{SSL} \cdot 2 \cdot F} + J_{diff} \frac{V_{PCS}}{V_{SSL}} - J_{SERCA,s} \cdot \frac{V_{NSR}}{V_{SSL}} - J_{gap}$$

$$TRPN_{SSL} = \overline{TRPN}_{SSL} \cdot \frac{[Ca^{2+}]_{SSL}}{[Ca^{2+}]_{SSL} + K_{m,TRPN}}$$

$$CMDN_{SSL} = \overline{CMDN}_{SSL} \cdot \frac{[Ca^{2+}]_{SSL}}{[Ca^{2+}]_{SSL} + K_{m,CMDN}}$$

$$[Ca^{2+}]_{SSL,tot} = [Ca^{2+}]_{SSL} + TRPN_{SSL} + CMDN_{SSL} + d[Ca^{2+}]_{SSL}$$

$$b_{SSL} = \overline{TRPN}_{SSL} + \overline{CMDN}_{SSL} - [Ca^{2+}]_{SSL,tot} + K_{m,TRPN} + K_{m,CMDN}$$

$$c_{SSL} = K_{m,TRPN} \cdot K_{m,CMDN} - [Ca^{2+}]_{SSL,tot} \cdot (K_{m,TRPN} + K_{m,CMDN}) + \overline{TRPN}_{SSL} \cdot K_{m,CMDN} + \overline{CMDN}_{SSL} \cdot K_{m,TRPN}$$

$$d_{SSL} = -K_{m,TRPN} \cdot K_{m,CMDN} \cdot [Ca^{2+}]_{SSL,tot}$$

$$[Ca^{2+}]_{SSL} = \frac{2}{3} \cdot \sqrt{b_{SSL}^2 - 3 \cdot c_{SSL}} \cdot \cos\left(\frac{1}{3} \cos^{-1}\left(\frac{9b_{SSL}c_{SSL} - 2b_{SSL}^3 - 27d_{SSL}}{2(b_{SSL}^2 - 3c_{SSL})^{1.5}}\right)\right) - \frac{b_{SSL}}{3}$$

○ $[Ca^{2+}]_i$ (Ca^{2+} concentration in Myo):

$$\frac{d[Ca^{2+}]_i}{dt} = J_{gap} \frac{V_{SSL}}{V_{Myo}} - J_{SERCA} \cdot \frac{V_{NSR}}{V_{Myo}} + J_{RyR_2} \frac{V_{CSR}}{V_{Myo}}$$

$$TRPN_{Myo} = \overline{TRPN}_{Myo} \cdot \frac{[Ca^{2+}]_i}{[Ca^{2+}]_i + K_{m,TRPN}}$$

$$CMDN_{Myo} = \overline{CMDN}_{Myo} \cdot \frac{[Ca^{2+}]_i}{[Ca^{2+}]_i + K_{m,CMDN}}$$

$$[Ca^{2+}]_{i,tot} = [Ca^{2+}]_i + TRPN_{Myo} + CMDN_{Myo} + d[Ca^{2+}]_i$$

$$b_{Myo} = \overline{TRPN}_{Myo} + \overline{CMDN}_{Myo} - [Ca^{2+}]_{i,tot} + K_{m,TRPN} + K_{m,CMDN}$$

$$c_{Myo} = K_{m,TRPN} \cdot K_{m,CMDN} - [Ca^{2+}]_{i,tot} \cdot (K_{m,TRPN} + K_{m,CMDN}) + \overline{TRPN}_{Myo} \cdot K_{m,CMDN} + \overline{CMDN}_{Myo} \cdot K_{m,TRPN}$$

$$d_{Myo} = -K_{m,TRPN} \cdot K_{m,CMDN} \cdot [Ca^{2+}]_{i,tot}$$

$$[Ca^{2+}]_i = \frac{2}{3} \cdot \sqrt{b_{Myo}^2 - 3 \cdot c_{Myo}} \cdot \cos\left(\frac{1}{3} \cos^{-1}\left(\frac{9b_{Myo}c_{Myo} - 2b_{Myo}^3 - 27d_{Myo}}{2(b_{Myo}^2 - 3c_{Myo})^{1.5}}\right)\right) - \frac{b_{Myo}}{3}$$

○ $[Ca^{2+}]_{JSR}$:

$$\frac{d[Ca^{2+}]_{JSR}}{dt} = J_{tr,j} - J_{RyR_3} - J_{IP_3R}$$

$$CSQN_{JSR} = \overline{CSQN}_{JSR} \cdot \frac{[Ca^{2+}]_{JSR}}{[Ca^{2+}]_{JSR} + K_{m,CSQN}}$$

$$b_{JSR} = \overline{CSQN}_{JSR} - CSQN_{JSR} - [Ca^{2+}]_{JSR} - d[Ca^{2+}]_{JSR} + K_{m,CSQN}$$

$$c_{JSR} = K_{m,CSQN} \cdot (\overline{CSQN}_{JSR} + [Ca^{2+}]_{JSR} + d[Ca^{2+}]_{JSR})$$

$$[Ca^{2+}]_{JSR} = \frac{(\sqrt{b_{JSR}^2 + 4c_{JSR}} - b_{JSR})}{2}$$

○ $[Ca^{2+}]_{CSR}$:

$$\frac{d[Ca^{2+}]_{CSR}}{dt} = J_{tr,c} - J_{RyR_2}$$

$$CSQN_{CSR} = \overline{CSQN}_{CSR} \cdot \frac{[Ca^{2+}]_{CSR}}{[Ca^{2+}]_{CSR} + K_{m,CSQN}}$$

$$b_{CSR} = \overline{CSQN}_{CSR} - CSQN_{CSR} - [Ca^{2+}]_{CSR} - d[Ca^{2+}]_{CSR} + K_{m,CSQN}$$

$$c_{CSR} = K_{m,CSQN} \cdot (\overline{CSQN}_{CSR} + [Ca^{2+}]_{CSR} + d[Ca^{2+}]_{CSR})$$

$$[Ca^{2+}]_{CSR} = \frac{(\sqrt{b_{CSR}^2 + 4c_{CSR}} - b_{CSR})}{2}$$

○ $[Ca^{2+}]_{NSR}$:

$$\frac{d[Ca^{2+}]_{NSR}}{dt} = J_{SERCA} + J_{SERCA,s} - J_{tr,c} \cdot \frac{V_{CSR}}{V_{NSR}} - J_{tr,j} \cdot \frac{V_{JSR}}{V_{NSR}}$$

○ $[Na^{2+}]_{PCS}$:

$$J_{diff,Na} = \frac{[Na^+]_{PCS} - [Na^+]_{SSL}}{\tau_{diff}}$$

$$J_{gap,Na} = \frac{[Na^+]_{SSL} - [Na^+]_i}{\tau_{gap}}$$

$$\frac{d[Na^{2+}]_{PCS}}{dt} = -3 \cdot I_{NaCa,PCS} \cdot \frac{A_{Cap}}{V_{PCS} \cdot z_{Na} \cdot F} - J_{diff,Na}$$

○ $[Na^{2+}]_{SSL}$:

$$\frac{d[Na^{2+}]_{SSL}}{dt} = -3 \cdot I_{NaCa,SSL} \cdot \frac{A_{Cap}}{V_{SSL} \cdot z_{Na} \cdot F} + J_{diff,Na} \cdot \frac{V_{PCS}}{V_{SSL}} + CT_{NaCl} - J_{gap,Na}$$

In the following (and throughout), subscript "i" indicates the myoplasmic compartment (Myo).

○ $[Na^{2+}]_i$:

$$\frac{d[Na^{2+}]_i}{dt} = -J_{gap,Na} \cdot \frac{V_{SSL}}{V_{Myo}}$$

○ $[K^+]_i$:

$$\frac{d[K^+]_i}{dt} = -I_{K,tot} \cdot \frac{A_{Cap}}{(V_{SSL} + V_{Myo} + V_{PCS}) \cdot z_K \cdot F}$$

Calcium/Calmodulin-Dependent Protein Kinase (CAMKII)

The CAMK model is equivalent to that used in the HRd model⁹. We assume that CAMK kinetics are similar in Purkinje and ventricular cells.

$$\alpha_{CAMK} = 0.05 \text{ ms}^{-1}; \beta_{CAMK} = 0.00068 \text{ ms}^{-1};$$

$$CAMK_0 = 0.05; K_{mCaM} = 0.0015 \text{ mM}$$

$$\frac{dCAMK_{trap}}{dt} = \alpha_{CAMK} \cdot CAMK_{bound} \cdot (CAMK_{bound} + CAMK_{trap}) - \beta_{CAMK} \cdot CAMK_{trap}$$

$$CAMK_{bound} = CAMK_0 \cdot \frac{1 - CAMK_{trap}}{1 + \frac{K_{mCaM}}{[Ca^{2+}]_{PCS}}}$$

$$CAMK_{active} = CAMK_{bound} + CAMK_{trap}$$

Cell Geometry

Purkinje cell geometry is determined based on experimental measurements of isolated canine Purkinje cells³². The subcellular compartments and their volumes are based on the histological studies by Sommer and Johnson³³. Due to lack of t-tubular network, R_{CG} (ratio of capacitive to geometric area) is set to 1.54²² (instead of 2 in the HRd ventricular cell model).

Length (L) = 0.0164 cm; radius (r) = 0.00175 cm

Cell volume: $V_{cell} = \pi \cdot r^2 \cdot L = 1.57 \times 10^{-4} \mu L$

Geometric membrane area: $A_{geo} = 2 \cdot \pi \cdot r^2 + 2 \cdot \pi \cdot L = 1.9957 \times 10^{-4} cm^2$

Capacitive membrane area: $A_{cap} = R_{CG} \cdot A_{geo} = 1.9957 \times 10^{-4} cm^2$

Myoplasm volume: $V_{Myo} = V_{cell} \cdot 60\%$

Mitochondria volume: $V_{mito} = V_{cell} \cdot 18\%$

SR volume: $V_{SR} = V_{cell} \cdot 5\%$

NSR volume: $V_{NSR} = V_{cell} \cdot 4\%$

JSR volume: $V_{JSR} = V_{cell} \cdot 0.2\%$

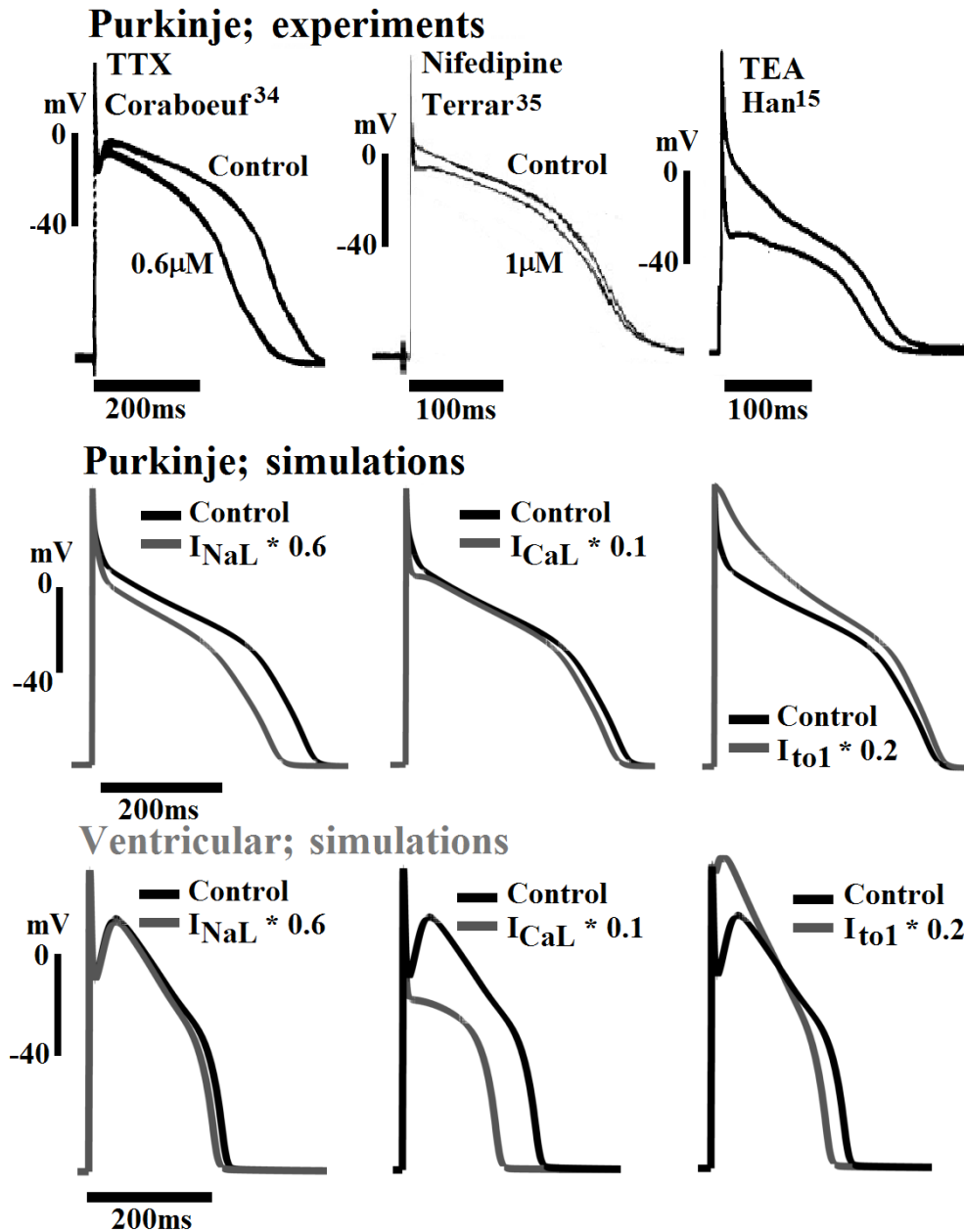
CSR volume: $V_{CSR} = V_{cell} \cdot 0.8\%$

Peripheral coupling subspace volume: $V_{PCS} = V_{cell} \cdot 2\%$

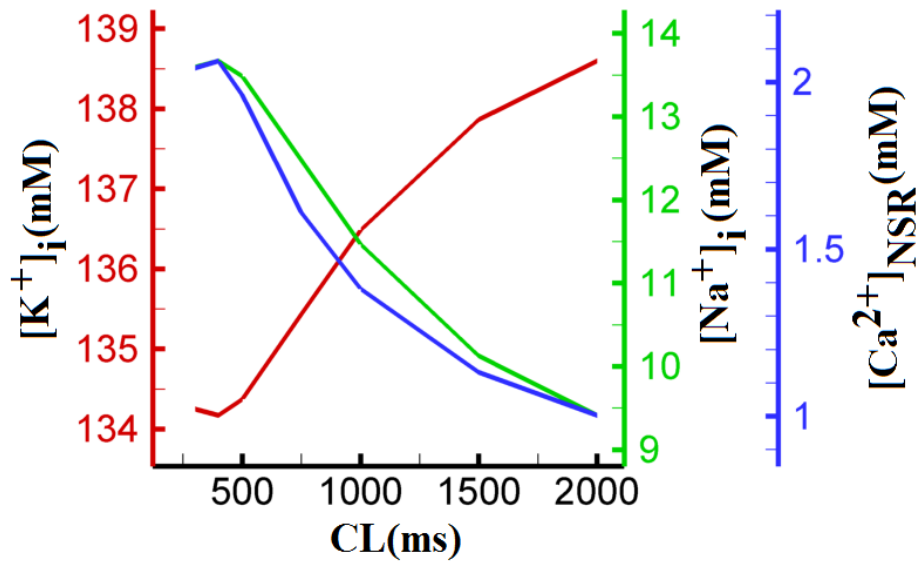
Subsarcolemmal region volume: $V_{SSL} = V_{cell} \cdot 15\%$

Species Specificity

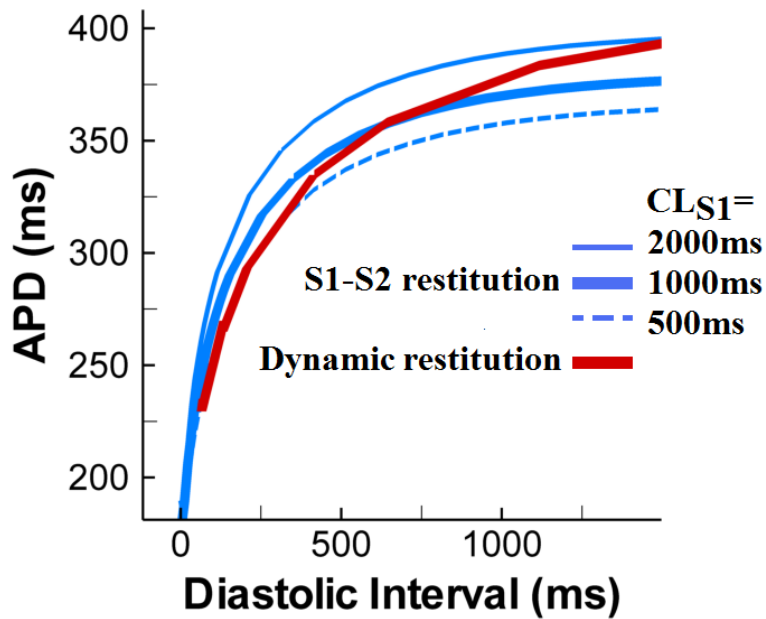
Purkinje cell electrophysiologic properties are species dependent³⁹. Given the availability of experimental data from canine Purkinje fibers or cells, our model is constructed to be canine-specific.



Online Figure VIII. Drug effects on Purkinje AP during pacing at CL=1000ms. Response to TTX (blocker of I_{NaL}), Nifedipine (blocker of I_{CaL}) and TEA (blocker of I_{to1}) are shown (left to right). Experimental data are shown in top panels. Middle and bottom panels show simulations in Purkinje and ventricular cell, respectively.



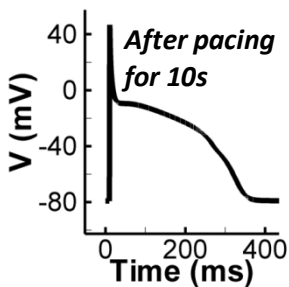
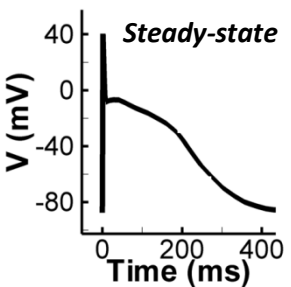
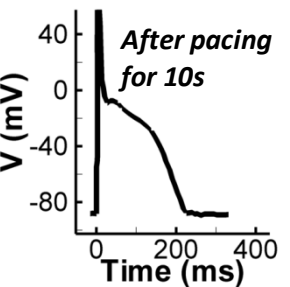
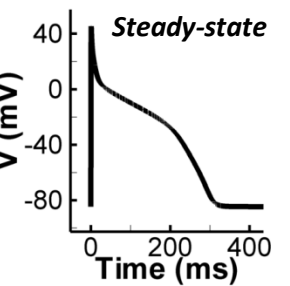
Online Figure IX. Simulated rate dependence of intracellular K^+ (red), Na^+ (green) and SR Ca^{2+} (blue) in Purkinje cell.

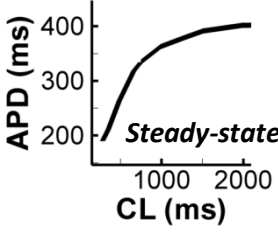
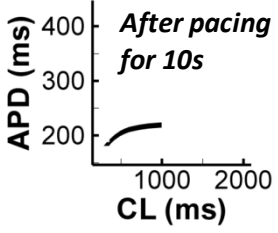
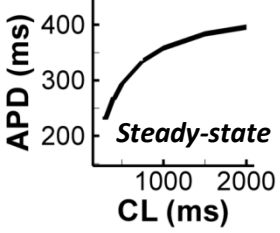
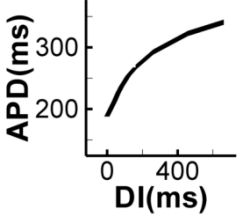
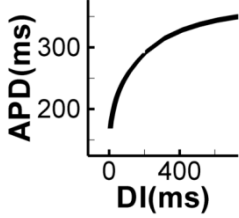


Online Figure X. Simulated S1-S2 (blue) and dynamic (red) APD restitution curves for Purkinje cell. The dynamical restitution curve is generated by plotting steady-state APD against steady-state DI at different pacing CLs.

V MODELS COMPARISON TABLE

The table below presents an overview of recent computational models³⁶⁻³⁸ of cardiac Purkinje cells. Model properties are obtained from performing computer simulations^{36,37} or from the literature³⁸. H-H, Hodgkin-Huxley formalism; SR, sarcoplasmic reticulum; NSR, network SR; JSR, junctional SR; CSR, corbular SR; PCS, peripheral coupling subspace; SSL, sub-sarcolemmal region; Myo, myoplasm; RyR, ryanodine receptor; RyR2, type 2 RyR; RyR3, type 3 RyR; IP3R, inositol trisphosphate receptor; G_{CaL} , conductance of L-type calcium channel; DI, diastolic interval.

| Study | Aslanidi et al Biophys J 2009 [36]* | Sampson et al J Physiol 2010 [37]* | Corrias et al AJP 2011 [38]# | PRd (Present study) |
|--|---|---|--|--|
| <i>Species</i> | Canine | Human | Rabbit | Canine |
| <i>Model Formulation</i> | H-H | Markov; H-H | H-H | H-H |
| <i>Subcellular Ca²⁺ Compartments</i> | 4 (NSR, JSR, Subspace, Myo) | 4 (NSR, JSR, Subspace, Myo) | 3 (Peripheral Myo, bulk Myo, SR) | 6 (NSR, JSR, CSR, PCS, SSL, Myo) |
| <i>Purkinje-specific Ca²⁺ Cycling</i> | No | No | Yes | Yes |
| <i>Steady-State</i> | No | Yes | N/A ^a | Yes |
| <i>SR Ca²⁺ Release</i> | SR Ca ²⁺ release to Subspace | Ca ²⁺ release via RyR to Subspace | SR Ca ²⁺ release to Peripheral Myo | Ca ²⁺ release via RyR3 and IP ₃ R to PCS; Ca ²⁺ release via RyR2 to Myo |
| <i>CaMKII Signaling</i> | Yes | No | No | Yes |
| <i>AP Morphology (CL=500ms)</i> |  |  |  |  |

| | | | | |
|--|------------------|---|--|---|
| APD Rate Adaptation | N/A ^b |  |  |  |
| APD Restitution | N/A ^b |  | N/A ^c |  |
| AP and Ca²⁺ Alternans (CL=200ms) | Yes | No | N/A ^c | Yes |
| EAD | No ^d | No ^d | Yes ^e | Yes ^d |

^aSimulation results of APD rate adaptation in Corrias et al³⁸ are provided after pacing for 10s.

^bNot available since the model presented in Aslanidi et al³⁶ cannot reach steady state.

^cNot provided in Corrias et al³⁸.

^dSimulation protocol: CL = 4000ms; initial $[Ca^{2+}]_{NSR} = 1.0mM/L$; initial $[Na^+]_i = 8.0mM/L$; complete block of I_{Kr} .

^eSimulation protocol: increased I_{CaL} conductance; $G_{CaL} \times 3.5$, CL-N/A³⁸

VI SUPPLEMENTAL REFERENCES

1. Han W, Chartier D, Li D, Nattel S. Ionic remodeling of cardiac Purkinje cells by congestive heart failure. *Circulation*. 2001;104:2095.
2. Shah AK, Cohen IS, Dattner NB. Background K^+ current in isolated canine cardiac Purkinje myocytes. *Biophysical journal*. 1987;52:519-525.
3. Herron TJ, Milstein ML, Anumonwo J, Priori SG, Jalife J. Purkinje Cell Calcium Dysregulation Is the Cellular Mechanism that Underlies Catecholaminergic Polymorphic Ventricular Tachycardia. *Heart Rhythm*. 2010;7:1122-8
4. Lee CO, Dagostino M. Effect of Strophanthidin on Intracellular Na ion Activity and Twitch Tension of Constantly Driven Canine Cardiac Purkinje Fibers. *Biophysical journal*. 1982;40:4.
5. Hess P, Wier WG. Excitation-contraction coupling in cardiac Purkinje fibers. Effects of caffeine on the intracellular $[Ca^{2+}]$ transient, membrane currents, and contraction. *The Journal of general physiology*. 1984;83:417.
6. Boyden PA, Pu J, Pinto J, Keurs H. Ca^{2+} transients and Ca^{2+} waves in Purkinje cells: role in action potential initiation. *Circulation research*. 2000;86:448.
7. Balati V. Comparison of the cellular electrophysiological characteristics of canine left ventricular epicardium, M cells, endocardium and Purkinje fibres. *Acta Physiologica Scandinavica*. 1998;164:181-190.
8. Elharrar V, Atarashi H, Surawicz B. Cycle length-dependent action potential duration in canine cardiac Purkinje fibers. *American Journal of Physiology- Heart and Circulatory Physiology*. 1984;247:H936.
9. Decker KF, Heijman J, Silva JR, Hund TJ, Rudy Y. Properties and ionic mechanisms of action potential adaptation, restitution, and accommodation in canine epicardium. *American Journal of Physiology- Heart and Circulatory Physiology*. 2009;296:H1017.
10. Bocchi L, Vassalle M. Characterization of the slowly inactivating sodium current I_{Na2} in canine cardiac single Purkinje cells. *Experimental physiology*. 2008;93:347-361.
11. Rota M, Vassalle M. Patch-clamp analysis in canine cardiac Purkinje cells of a novel sodium component in the pacemaker range. *The Journal of Physiology*. 2003;548:147.
12. Hirano Y, Fozzard HA, January CT. Characteristics of L- and T-type Ca^{2+} currents in canine cardiac Purkinje cells. *American Journal of Physiology-Heart and Circulatory Physiology*. 1989;256:H1478.
13. Tseng GN, Boyden PA. Multiple types of Ca^{2+} currents in single canine Purkinje cells. *Circulation research*. 1989;65:1735.
14. Dumaine R, Cordeiro JM. Comparison of K^+ currents in cardiac Purkinje cells isolated from rabbit and dog. *Journal of molecular and cellular cardiology*. 2007;42:378-389.
15. Han W, Wang Z, Nattel S. A comparison of transient outward currents in canine cardiac Purkinje cells and ventricular myocytes. *American Journal of Physiology- Heart and Circulatory Physiology*. 2000;279:H466.
16. Stewart P, Aslanidi OV, Noble D, Noble PJ, Boyett MR, Zhang H. Mathematical models of the electrical action potential of Purkinje fibre cells. *Philosophical Transactions of the Royal Society A: Mathematical, Physical and Engineering Sciences*. 2009;367:2225.
17. Maltsev VA, Lakatta EG. A novel quantitative explanation for the autonomic modulation of cardiac pacemaker cell automaticity via a dynamic system of sarcolemmal and intracellular proteins. *American Journal of Physiology- Heart and Circulatory Physiology*. 2010;298:H2010.
18. Jeck C, Pinto J, Boyden P. Transient outward currents in subendocardial Purkinje myocytes surviving in the infarcted heart. *Circulation*. 1995;92:465.
19. Altomare C, Bucchi A, Camatini E, Baruscotti M, Viscomi C, Moroni A, DiFrancesco D. Integrated allosteric model of voltage gating of HCN channels. *The Journal of General Physiology*. 2001;117:519.

20. Han W, Bao W, Wang Z, Nattel S. Comparison of ion-channel subunit expression in canine cardiac Purkinje fibers and ventricular muscle. *Circulation research*. 2002;91:790.
21. Yu H, Chang F, Cohen IS. Pacemaker current i_f in adult canine cardiac ventricular myocytes. *The Journal of Physiology*. 1995;485:469.
22. Cohen IS, Datyner NB, Gintant GA, Mulrine NK, Pennefather P. Properties of an electrogenic sodium-potassium pump in isolated canine Purkinje myocytes. *The Journal of Physiology*. 1987;383:251.
23. Gao J, Wang W, Cohen IS, Mathias RT. Transmural gradients in Na/K pump activity and $[Na^+]_i$ in canine ventricle. *Biophysical journal*. 2005;89:1700-1709.
24. Gaborit N, Le Bouter S, Szuts V, Varro A, Escande D, Nattel S, Demolombe S. Regional and tissue specific transcript signatures of ion channel genes in the non diseased human heart. *The Journal of Physiology*. 2007;582:675-693.
25. Dun W, Boyden PA. The Purkinje cell; 2008 style. *Journal of molecular and cellular cardiology*. 2008;45:617-624.
26. Boyden PA, Albala A, Dresdner Jr KP. Electrophysiology and ultrastructure of canine subendocardial Purkinje cells isolated from control and 24-hour infarcted hearts. *Circulation research*. 1989;65:955.
27. Livshitz LM, Rudy Y. Regulation of Ca^{2+} and electrical alternans in cardiac myocytes: role of CAMKII and repolarizing currents. *American Journal of Physiology- Heart and Circulatory Physiology*. 2007;292:H2854.
28. Stuyvers BD, Dun W, Matkovich S, Sorrentino V, Boyden PA, ter Keurs H. Ca^{2+} sparks and waves in canine purkinje cells: a triple layered system of Ca^{2+} activation. *Circulation research*. 2005;97:35.
29. Lado MG, Sheu SS, Fozzard HA. Changes in intracellular Ca^{2+} activity with stimulation in sheep cardiac Purkinje strands. *American Journal of Physiology-Heart and Circulatory Physiology*. 1982;243:H133.
30. Bugrim AE, Zhabotinsky AM, Epstein IR. Calcium waves in a model with a random spatially discrete distribution of Ca^{2+} release sites. *Biophysical journal*. 1997;73:2897-2906.
31. De Young GW, Keizer J. A single-pool inositol 1, 4, 5-trisphosphate-receptor-based model for agonist-stimulated oscillations in Ca^{2+} concentration. *Proceedings of the National Academy of Sciences of the United States of America*. 1992;89:9895.
32. Sheets MF, January CT, Fozzard HA. Isolation and characterization of single canine cardiac purkinje cells. *Circulation research*. 1983;53:544.
33. Sommer JR, Johnson EA. Cardiac muscle. *The Journal of Cell Biology*. 1968;36:497.
34. Coraboeuf E, Deroubaix E, Coulombe A. Effect of tetrodotoxin on action potentials of the conducting system in the dog heart. *American Journal of Physiology- Heart and Circulatory Physiology*. 1979;236:H561.
35. Terrar DA, Wilson CM, Graham SG, Bryant SM, Heath BM. Comparison of guinea-pig ventricular myocytes and dog Purkinje fibres for in vitro assessment of drug-induced delayed repolarization. *Journal of pharmacological and toxicological methods*. 2007;56:171-185.
36. Aslanidi OV, Sleiman RN, Boyett MR, Hancox JC, Zhang H. Ionic Mechanisms for Electrical Heterogeneity between Rabbit Purkinje Fiber and Ventricular Cells. *Biophysical journal*. 2009;98:2420-2431.
37. Sampson KJ, Iyer V, Marks AR, Kass RS. A computational model of Purkinje fibre single cell electrophysiology: implications for the long QT syndrome. *The Journal of physiology*. 588:2643.
38. Corrias A, Giles WR, Rodriguez B. Ionic mechanisms of electrophysiological properties and repolarization abnormalities in rabbit Purkinje fibers. *American Journal of Physiology-Heart and Circulatory Physiology*. 2011;doi: 10.1152/ajpheart.01170.2010
39. Lu HR, Marien R, Saels A, Clerck F. Species Plays an Important Role in Drug Induced Prolongation of Action Potential Duration and Early Afterdepolarizations in Isolated Purkinje Fibers. *Journal of cardiovascular electrophysiology*. 2001;12:93-102.